applied sciences

MDPI

Article

A Porous Media Model for the Numerical Simulation of Acoustic Attenuation by Perforated Liners in the Presence of Grazing Flows

Jianguo Wang [1,*], Philip Rubini [2] and Qin Qin [2]

[1] Jiangsu (Sunpower) Research Institute of Industrial Energy Saving Technology, Jiangsu Sunpower Technology Co. Ltd., Nanjing 210000, China
[2] School of Engineering and Computer Science, University of Hull, Kingston upon Hull HU6 7RX, UK; p.a.rubini@hull.ac.uk (P.R.); q.qin@hull.ac.uk (Q.Q.)
* Correspondence: wangjianguo@sunpower.com.cn

Featured Application: Passive control devices for combustion noise reduction in gas turbine engines and/or other general flow noises.

Abstract: In this paper, a novel model is proposed for the numerical simulation of noise-attenuating perforated liners. Effusion cooling liners offer the potential of being able to attenuate combustion instabilities in gas turbine engines. However, the acoustic attenuation of a perforated liner is a combination of a number of interacting factors, resulting in the traditional approach of designing perforated combustor liners relying heavily on combustor rig tests. On the other hand, direct computation of thousands of small-scale holes is too expensive to be employed as an engineering design tool. In recognition of this, a novel physical velocity porous media (PVPM) model was recently proposed by the authors as a computationally less demanding approach to represent the acoustic attenuation of perforated liners. The model was previously validated for the normal incidence of a sound wave by comparison with experimental data from impedance tubes. In this paper, the model is further developed for configurations where the noise signal propagates in parallel with the perforated liners, both in the presence and absence of a mean flow. The model is significantly improved and successfully validated within coexisting grazing and bias flow scenarios, with reference to a series of well-recognized experimental data.

Keywords: perforated liners; acoustic damping; porous media model; acoustic passive control; numerical simulation; combustion instability; effusion cooling walls

Citation: Wang, J.; Rubini, P.; Qin, Q. A Porous Media Model for the Numerical Simulation of Acoustic Attenuation by Perforated Liners in the Presence of Grazing Flows. *Appl. Sci.* **2021**, *11*, 4677. https://doi.org/10.3390/app11104677

Academic Editor: Francesca Scargiali

Received: 21 April 2021
Accepted: 17 May 2021
Published: 20 May 2021

1. Introduction

In gas turbine engines, NOx emissions can be reduced through the use of lean premixed combustion technologies (LPC) [1]. In contrast to traditional non-premixed combustion, lean premixed combustion processes are more susceptible to combustion instability [2,3]. In the gas turbine industry, Helmholtz resonators and perforated combustor liner absorbers are two common approaches that have been adopted to attenuate large amplitude pressure oscillations in gas turbine combustors [4–6]. Helmholtz resonators are able to provide very high attenuation at their resonant frequency. Perforated combustor liners were originally conceived as a means to provide enhanced cooling of gas turbine liners [7]. However, with the appropriate design, they are not only lighter and more compact but they also offer the potential to attenuate pressure fluctuations over a much broader frequency range compared to single-neck Helmholtz resonators [8,9].

A number of parameters impact the ability of perforated wall liners to attenuate pressure fluctuations. Geometric factors include the liner geometry [10–12], liner thickness [13,14] and the shape of the cavity [15–17]. Flow parameters include the sound

pressure level [18–20], bias flow and grazing flow velocity [21–24] and temperature of the grazing flow [25–27]. Attenuation performance also depends on periphery acoustic boundary conditions including incident angles and the size of perforated liners [28].

From a computational perspective, detailed resolution of the very large number of small-scale effusion cooling holes is computationally too expensive as a practical engineering tool [29–31]. Simple empirical models are unable to predict acoustic attenuation by a perforated liner over a broad range of applications, resulting in the continued reliance upon traditional experimental techniques.

Jianguo et al. [32] proposed that a perforated wall can be represented by a homogeneous physical velocity porous media model (PVPM model), rendering detailed resolution of the perforations unnecessary. The model was demonstrated to be able to account for flow pressure drops across the liner and, through extensive validation, was shown to be able to accurately capture acoustic damping effects in a range of normal incidence conditions. The model was validated both for linear and non-linear damping regimes and in bias flows where inertial effects are dominant.

The model of Jianguo et al. [32] was, however, only validated for the normal incidence of a sound wave, consequently restricting the range of practical application. In this paper, the model is further extended to the following:

- Where the noise signal propagates in parallel with a perforated liner without a mean flow;
- Where the noise signal propagates in parallel with a perforated liner in the presence of a mean bias flow;
- Where the noise signal propagates in parallel with a perforated liner in the presence of a mean grazing flow;
- Where the noise signal propagates in parallel with a perforated liner in the presence of coexisting bias and grazing flows;
- Where the grazing flow is of higher temperatures.

2. Methods

The validation of the current model was conducted by firstly carrying out self-designed experiments and also selecting a series of the most cited and recognized experimental works in the relevant scope, and, finally, by providing a direct comparison between the modeling results and those benchmark experimental data. For experimental methods, data processing methods and mesh independence studies, please refer to the related references and also the authors' previous publication [8,32]. This section will focus on how the PVPM model was further developed on the foundation of the previous work [32].

2.1. Background Theory

Computational fluid dynamics (CFD) is based upon the numerical solution of the underlying governing equations for a fluid flow, under specified boundary conditions. The propagation of an acoustic wave in a flow tube may be represented as an unsteady three-dimensional compressible flow, and the corresponding governing equations may be expressed in three-dimensional Cartesian coordinates as [33]

Mass conservation equation:

$$\frac{\partial \rho}{\partial t} + \operatorname{div}\left(\rho \vec{u}\right) = 0 \tag{1}$$

Momentum conservation:

$$\frac{\partial (\rho u)}{\partial t} + \operatorname{div}\left(\rho u \vec{u}\right) = -\frac{\partial p}{\partial x} + \operatorname{div}(\tau_{ix}) + S_{Mx} \tag{2}$$

$$\frac{\partial (\rho v)}{\partial t} + \operatorname{div}\left(\rho v \vec{u}\right) = -\frac{\partial p}{\partial y} + \operatorname{div}(\tau_{iy}) + S_{My} \tag{3}$$

$$\frac{\partial(\rho w)}{\partial t} + \operatorname{div}\left(\rho w \vec{\mathrm{u}}\right) = -\frac{\partial p}{\partial z} + \operatorname{div}(\tau_{iz}) + S_{Mz} \tag{4}$$

where u, v, w are the components of the velocity vector $\vec{\mathrm{u}}$ in x, y, z directions, respectively; τ_{ij} represents a viscous stress in the j direction exerted on a surface perpendicular to the i direction; S_M is the momentum source term to include other sources or sinks of the momentum such as body forces; ρ, p are, respectively, the density and pressure of the fluid; and t is the time.

Energy equation:

$$\frac{\partial(\rho h)}{\partial t} + \operatorname{div}\left(\rho h \vec{\mathrm{u}}\right) = \operatorname{div}(k \operatorname{grad} T) + \frac{\partial p}{\partial t} + \operatorname{div}\left(\tau_{ij} \vec{\mathrm{u}}\right) + S_h \tag{5}$$

where h represents the specific total enthalpy, k is thermal conductivity, S_h is the enthalpy source term and T is the temperature. The ideal gas equation of state is applied to determine the density of the fluid.

The PVPM model was originally developed for the representation of uniform and highly porous materials, with a rigid frame. The model introduced a porosity term, σ, into the governing equations [33]. For example, when considering only the x direction within a porous zone, the continuity and momentum equations may be written as

$$\frac{\partial(\sigma\rho)}{\partial t} + \operatorname{div}\left(\sigma\rho \vec{\mathrm{u}}\right) = 0 \tag{6}$$

$$\frac{\partial(\rho\sigma u)}{\partial t} + \operatorname{div}\left(\rho\sigma u \vec{\mathrm{u}}\right) = -\sigma\frac{\partial p}{\partial x} + \operatorname{div}(\sigma\tau_{ix}) + \sigma S_{Mx} \tag{7}$$

Porosity σ is defined as the ratio of the void space to the overall bounding volume for the plate. u is the x direction velocity. The magnitude of the velocity vector $\vec{\mathrm{u}}$ within the porous region has to be amplified by a factor $1/\sigma$ for the transverse flow to satisfy the mass continuity. This resultant physical velocity is equivalent to the average real velocity within the porous material region. Therefore, mass flow rate conservation and the correct representation of the overall velocity changes across the porous region are simultaneously achieved by applying the physical velocity porous media model, which makes the acquisition of acoustic properties possible. S_{Mx} is the pressure source term for the PVPM model and $S_{Mx} = \frac{\Delta P}{l_{\text{eff}}} = \frac{\mu}{\alpha}u$, where l_{eff} is the effective thickness of the porous media zone which will be described in Section 2.2.2, μ is the dynamic viscosity of the medium in which the sound signal propagates and α is the permeability of the porous media region. Since flow resistance r is defined as $r = \frac{\Delta P}{u}$, and in the PVPM model, $\frac{\Delta P}{u} = \frac{\mu}{\alpha}l_{\text{eff}}$, the parameter that needs to be defined in ANSYS Fluent 17.2 to accommodate the extra flow resistance as described in Section 2.2.1 is essentially a parameter called inverse permeability $\frac{1}{\alpha}$ [33], which can be obtained by combining the above two equations $\frac{1}{\alpha} = \frac{r}{\mu l_{\text{eff}}}$.

On the other hand, the PVPM model represents a perforated liner as a homogenous material without the necessity of resolving small-scale details of the perforation. The model was successfully validated by Jianguo et al. [32] against a number of highly cited papers reporting experiments in impedance tubes, where the acoustic signal was incident normal to the perforated liner. Jianguo et al. [32] demonstrated that the PVMP model was able to represent the acoustic attenuation of perforated liner absorbers in both the linear and non-linear damping regimes and also the inertial damping effect in the presence of a mean bias flow.

In the PVPM model proposed by Jianguo et al. [32], the pressure loss due to viscous effects is directly related to the geometry of perforations, and this is inevitably lost by the homogenous geometry assumption. In cases without a mean bias flow, the viscous resistance is important and is included as a viscous resistance term in the pressure loss source term in S_M in Equation (7). The so-called acoustic end correction effect also cannot be directly represented by the homogenous porous model. In this case, the thickness of the

porous media region is defined to be the effective acoustic thickness of a perforated liner according to Equation (8) [32]:

$$l_{\text{eff}} = l_{\text{t}} + 0.85d\,\Psi\left(1 + \frac{\text{M}}{\sigma}\right)^{-1} \tag{8}$$

where l_{t} is the real liner thickness, d is the diameter of perforations,

$$\Psi = 1 - 1.4092\sqrt{\sigma} + 0.33818\sigma^{1.5} + 0.06793\sigma^{2.5} \tag{9}$$

represents the hole–hole interaction effect according to Fok's function Ψ [34] and M is the neck particle Mach number which accounts for both the bias mean flow and the acoustic pressure-induced acoustic flow:

$$\text{M} = \frac{\left[\text{U}_{\text{b}} + \sqrt{2}\text{RMS}(\text{U}_{\text{ac}})\right]}{c} \tag{10}$$

where U_{b} is the bias flow velocity and U_{ac} represents the acoustic velocity inside the perforations [32].

The original PVPM model was validated for cases where the noise signals and bias flow are normal to a perforated wall [32]. However, in many industrial applications, such as gas turbine combustors or automotive noise mufflers, noise signals and flows are often coincident and parallel to the perforated walls. In this section, the PVPM model is further developed for situations where perforated liners are exposed to grazing flows and also a simultaneous grazing/bias flow.

2.2. Further Development of PVPM Model

2.2.1. Extra Flow Resistance Due to Grazing Flow Effect

A grazing flow is a flow which travels in parallel with a perforated surface. A grazing flow impacts on the edges of perforations, creating local flow phenomena, as illustrated in Figure 1 [35]. The non-uniform flow in the region of the neck of the hole alters the flow resistance of the liner due to inertial losses. However, the extra inertial resistance due to non-uniform neck flows is not directly represented by the homogeneous porous media model. This must be taken into account by incorporating an additional flow resistance in the pressure drop source terms for the porous media region (see Equation (7)).

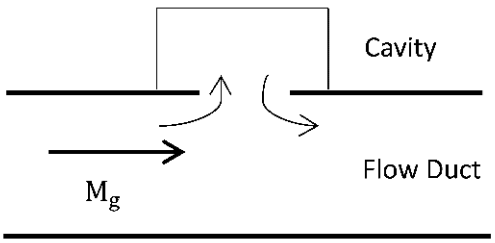

Figure 1. Illustration of a grazing flow-induced neck flow in a single perforation.

According to a series of experiments [36–40], the specific flow resistance r_{g} caused by grazing flows is proportional to the grazing flow Mach number M_{g}:

$$\text{r}_{\text{g}} = \frac{\text{C}_{\text{g}} \cdot \text{M}_{\text{g}}}{\sigma} \tag{11}$$

The proportional constant C_g is different across different experiments. C_g was claimed to be between 0.3 and 0.5 in these experiments. Heidelberg et al. [40] further confirmed that the coefficient C_g varies with the dimensions of perforations and, according to him,

$$r_g = \frac{M_g}{\sigma} / \left(2 + 1.256\frac{\delta}{d}\right) \tag{12}$$

where δ is the boundary layer thickness displacement due to grazing flow incidence. Syed et al. [37] found that δ is approximately 1.45 mm and hardly changes with strong grazing flow speeds. Therefore, grazing flow-induced normalized specific flow resistance of the porous media region is treated in this paper as

$$r_g = \frac{M_g}{\sigma} / \left(2 + \frac{0.0018}{d}\right) \tag{13}$$

The constant $C_g = 1/\left(2 + \frac{0.0018}{d}\right)$ varies from 0.5 for large perforations to 0.25 for small perforations. This variation in the grazing flow stirring effect with orifice sizes is intuitively understandable, where a stronger local neck flow will be created in a larger perforation due to the larger orifice open to impact by the grazing flow.

Grazing flows and bias flows coexist in the perforated liner of a gas turbine combustion chamber. A number of experiments [9,41,42] reported that the grazing flow is important only when the mean bias flow through the neck is relatively weak. Lahiri [9] found that the grazing flow and bias flow enhance noise damping effects to the same degree when $M_b/M_g = 1/3$ and the effect of the grazing flow can be ignored if $M_b/M_g > 1/3$. Similarly, Rice [41] proposed the ratio M_b/M_g to be 0.3, above which the grazing flow effect is negligible. Otherwise, when the grazing flow is much stronger than the bias flow, grazing flow-induced resistance is dominant over bias flow-induced resistance. Both Lahiri [9] and Rice [41] indicated that the overall flow resistance of a perforated liner is dominant either by the bias flow or the grazing flow, and it is sensible to take the larger resistance to be the resistance of the liner.

Bias flow-induced flow resistance, r_b, is directly resolved and accounted for by the current PVPM model, as discussed by Jianguo et al. [32]. The flow resistance due to a bias flow does not need to be imposed in the pressure loss source terms. However, the effect of grazing flows was not included in the original homogenous PVPM model. As a consequence, the overall flow resistance r of a perforated liner represented by the PVPM model is required to be amended by the grazing flow-induced resistance, as shown in Equation (14):

$$r = \begin{cases} 0 & \text{if } r_b \geq \frac{C_g M_g}{\sigma} \\ \frac{C_g M_g}{\sigma} - r_b & \text{if } r_b < \frac{C_g M_g}{\sigma} \\ \frac{C_g M_g}{\sigma} & \text{if } r_b = 0 \end{cases} \tag{14}$$

where $C_g = 1/(2 + 0.0018/d)$ according to Equation (13), and r_b is the bias flow-induced resistance for the porous media region which is resolved by the PVPM model [32].

2.2.2. Extra Porous Media Region Thickness Corrections Due to Grazing Flows

The effective acoustic thickness of a perforated liner is larger than the actual physical thickness due to the acoustic radiation effect at the end of the individual perforations. However, the original porous media model ignored such geometry details, and, as a result, the additional thickness due to the end radiation effect is lost. Therefore, when using the PVPM model in a numerical simulation, the thickness of the porous media region is required to be the effective acoustic thickness of the liner rather than the real liner thickness.

In the presence of significant acoustic pressure fluctuations and strong bias flows, the acoustic end correction length of a perforation is reduced [32]. A number of experiments found that the acoustic end correction length is reduced by the presence of grazing flows.

Rice [41] proposed a correction factor of $1/\left(1+305M_g^3\right)$ for end radiation length correction due to grazing flows. However, this term significantly underestimates the effect of grazing flows according to some other researchers [23,43]. Elnady and Boden [43] introduced a grazing flow acoustic reactance term, $-0.3M_g/\sigma$. However, experiments by Kooi, Kirby and Kaji et al. [44,45] clearly showed that the acoustic reactance did not decrease linearly with the grazing flow Mach number, as suggested. According to Kirby and Cummings [24], the end correction length starts to decline within moderate grazing flows, and the decrease in the end correction length slows down with increasing grazing flow speed. Kaji et al. [45] found the same trend where the decrease in acoustic reactance with grazing flow speeds nearly stopped if $M_g > 0.15$.

Grazing flows reduce the effect of acoustic radiation, as represented by the end correction length, in two different ways. First, a grazing flow-induced local neck flow reduces the end correction length in the same way as with bias flows, as described in Equation (10). Second, a grazing flow "blows away" the acoustic radiation on that side of the liner. The correction factor due to the "blowing away effect" is slightly under 0.5 when the high-speed grazing flow ($M_g > 0.15$) blows away all acoustic radiations at the flow side and also some air mass in the internal rim of orifices. Therefore, on the basis of Equation (8), the effective thickness of perforated liners is thus proposed to be

$$l_{\text{eff}} = l_t + 0.85d\left(1-1.4\sqrt{\sigma}\right)/\begin{cases} 1+\frac{M_b}{\sigma} & if\ M_g = 0 \\ \left(1+10M_g\right)\left(1+\frac{M_b}{\sigma}\right), & if\ \ M_b/M_g > C_g \\ \left(1+10M_g\right)\left(1+\frac{C_gM_g}{\sigma}\right), & if\ M_b/M_g < C_g \end{cases} \tag{15}$$

The term $\left(1+10M_g\right)$ considers the "blowing away" effect by the grazing flow. This term is no greater than 2.5 because the "blowing away" effect takes place only at the flow side of the liner and does not affect the acoustic radiation at the other side. The second term $\left(1+C_gM_g/\sigma\right)$ is to reflect the local neck flow effect, and this term will be replaced by $1+M_b/\sigma$ if the inertial resistance caused by bias flows is stronger than that due to grazing flows [45].

2.3. Numerical Schemes

The PVPM model was implemented in numerical simulations in ANSYS Fluent v17.2, employing the pressure-based segregated solver with pressure–velocity coupling achieved by the SIMPLE algorithm [33]. The discretized spatial terms were approximated by a second-order biased upwind scheme which provides both the numerical accuracy of a second-order upwind scheme and the convergence robustness of a first-order scheme. The turbulence terms were solved in a second-order upwind scheme. The discretized temporal terms were resolved using a bounded second-order accurate, implicit scheme, in order to robustly resolve the rapidly fluctuating pressure signal [35]. The working fluid was assumed to be air, described by the ideal gas equation of state.

Grazing flow and bias flow inlets were specified as mass flow inlet boundaries in the CFD simulations for which the mass flow rate is specified. Pressure outlet boundaries were employed to represent the grazing flow outlet. A general non-reflecting boundary condition proposed by Poinsot et al. [46,47] was applied where it was required to represent anechoic boundaries.

The perforated liner wall was represented with a homogenous plate zone and filled with 2–3 layers of a structured hexahedral mesh across its thickness, which significantly reduce the computational cell counts otherwise needed to represent the detailed hole structures. The solution time step was specified such that a minimum of 25 time steps were employed to resolve a time period of the physical input signal of the highest frequency. At least 25 layers of grid cells were defined to resolve one wavelength of the incident signal of the highest frequency. A viscous laminar flow was assumed for those cases where only an acoustic signal was present, or where a mean flow was present but the flow Reynolds

number was less than 3500. In those cases where the mean flow Reynolds number exceeded 3500, the standard $k-\varepsilon$ RANS turbulence model was enabled. In this work, all simulations were undertaken with the double precision version of ANSYS FLUENT 17.2 [33], as a three-dimensional, compressible, time-dependent flow.

2.4. Acoustic Data Processing Method

In this work, data from an in-house experiment and a number of highly cited publications were utilized to validate the further developed PVPM model. In these experiments, microphones were employed to record acoustic pressure fluctuations. The pressure data were further processed, and the acoustic impedance and the magnitude of any acoustic attenuation were derived. Three different acoustic data collection and processing methods exist: the two-microphone method [32], the four-microphone method [21] and an in situ impedance method [48]. The data processing method used in each experiment will be clarified in the Results section for each experiment. Static pressure monitors were defined in the CFD simulations at positions directly corresponding to where microphones were placed in the experiments to extract the acoustic wave information. The same data processing method as employed in the experimental work was then employed to process the pressure data to obtain the acoustic impedance or acoustic damping information. Acoustic impedance or acoustic damping information acquired by the numerical method and the experimental tests are presented in the following section in order to validate the proposed PVPM model.

3. Results

This section presents a step-by-step validation of the model within the different aforementioned scenarios. The acoustic properties of a series of perforated liners measured by the authors themselves and four well-acknowledged benchmark experiments are directly compared with those results acquired by the PVPM model using numerical methods.

3.1. Grazing Acoustic Signal without Flow

3.1.1. Self-Designed Experiment Configuration

Installation of a perforated liner could result in very different overall acoustic damping properties depending on the noise signal incidence angles [28]. In the previous work of the authors [32], the PVPM model was validated for situations where the fluctuating pressure was normal to the perforated plate. In the current paper, in order to validate the PVPM model in the noise signal grazing incidence conditions, an acoustic test rig, as shown in Figures 2 and 3, was constructed. The rig consists of an upstream duct section, a downstream duct section and a liner section installed in between them, each with an internal diameter of 165 mm. Four opposing loudspeakers were installed on the upstream duct. The test rig was designed to include anechoic terminations to minimize reflections from both ends. The pressure measurement uncertainty for those four microphones is within ±3%. In this test configuration, a mean flow is not present in the ducts or perforated liners, and other authors' experimental work is cited to validate the PVPM model in the presence of mean flows.

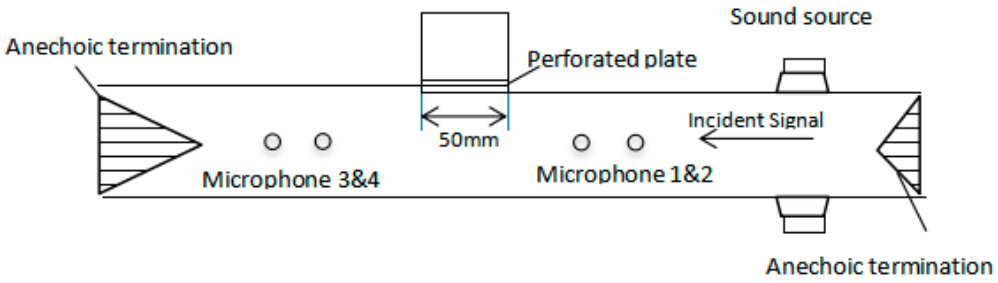

Figure 2. Experimental test rig setup.

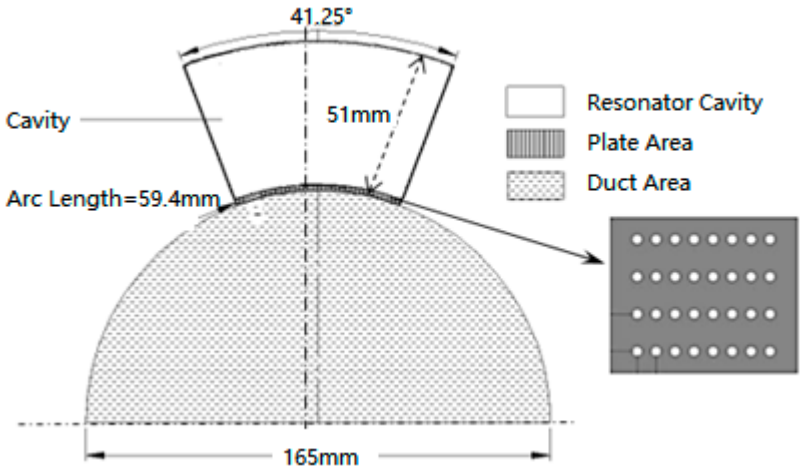

Figure 3. The position and shape of the perforated liner on the test rig.

A resonant cavity, Figure 3, was constructed from a 50 × 59.4 mm curved rectangular test liner, mounted flush to the side wall of the test section duct, with an attached fan-shaped cavity of 51 mm depth. The volume of the cavity is

$$V = \pi[(51\text{ mm} + 165 + 2\text{ mm})^2 - \left((165\text{ mm})/2 + 2\text{ mm})^2\right] \times \frac{41.25^\circ}{360^\circ} \times 50\text{ mm} = 201\text{ mL} \quad (16)$$

where 51 mm is the cavity depth, 165 mm is the internal diameter of the tube, 2 mm is the thickness of the liner and 41.25° represents the angle of the fan-shaped cavity. The cavity size is typical for distributed Helmholtz resonators installed on real gas turbines in order to attenuate noise within the combustor chamber.

A total of 32 circular perforations, as illustrated in Figure 3, were drilled in the curved liners. The diameters of these orifices ranged from 2 to 4 mm. In all cases, the thickness of the perforated plate was fixed at 2 mm. Detailed geometric features of the orifices are listed in Table 1.

Table 1. Geometry features of perforated liners H1, H2 and H3.

Liner No.	Hole Diameter (mm)	Liner Circumferential Length (mm)	Liner Axial length (mm)	Pitch-y (mm)	Pitch-x (mm)	Porosity σ
H1	2.0	59.4	50	6.0	12	0.0338
H2	3.0	59.4	50	6.0	12	0.0762
H3	4.0	59.4	50	6.0	12	0.135

A signal generator and amplifier were employed to generate a 100 dB noise signal within a bandwidth of 100–1000 Hz. Two pairs of microphones were installed in the upstream and downstream ducts, each pair separated by a distance of 10 cm. A four-microphone data processing method [21] was employed to process the data, and the acoustic absorption coefficients within the frequency range 100–1000 Hz were thereby obtained. Numerical simulations, with the PVPM model representing the liner region, were carried out to obtain the equivalent predicted acoustic absorption coefficients. The mesh distribution was as shown in Figure 4, where only two layers of structured meshes are applied to represent the thickness of the perforated liner, which significantly reduce the computational cost otherwise required to resolve the small holes [32].

The sound sources are two loudspeakers mounted perpendicular to the duct walls. With loudspeakers mounted on the side walls, their numerical representation can introduce an unrealistic flow disturbance due to interactions between the additional inlet and the incident grazing mean flow. In this work, the sound source was relocated to its neighboring mean flow inlets/outlet. The area of the acoustic signal inlet represented less than 1/10 of the overall area of the flow boundary so that the original acoustic impedance property of

this boundary was not affected. The acoustic signal was then introduced by superimposing the acoustic signal upon the mean flow. Care was taken to ensure that, regardless of the location of the sound source, the overall acoustic power matched that employed in the experiments.

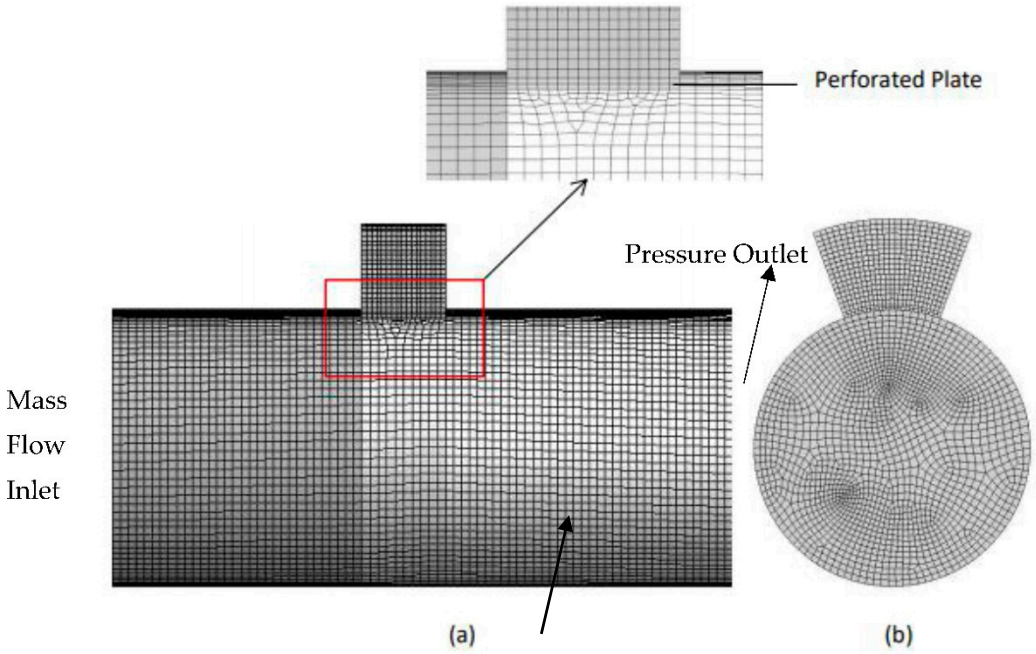

Figure 4. Mesh distribution for CFD simulations employing the PVPM model: (**a**) front view; (**b**) cross-sectional view.

3.1.2. Validation of the PVPM Model

Figure 5 compares CFD and experimental results of acoustic absorption coefficients for H1, H2 and H3 liner absorbers in the case of a grazing acoustic signal, but no mean flow. The numerical results and experimental results are, in general, in good agreement. Peak damping frequencies and the absorption bandwidth for all three perforated liner absorbers are well represented by the proposed PVPM model. Both numerical and experimental results show that peak absorption frequencies increase with increasing liner porosity. The liner H2 with 7.6% porosity displays the greatest peak attenuation effect.

Differences of up to 15% between the experimental and numerical results do exist, with the numerical results tending to overestimate the attenuation effect near the resonance frequencies for liner H1. The numerical results also tend to generate slightly narrower attenuation curves. This may indicate that the model slightly underestimates flow resistance induced by the grazing acoustic signal in the absence of a mean flow. This discrepancy could be further suppressed by including an additional flow resistance correction term accommodating the impact of a grazing acoustic flow. However, this impact is inappreciable in most conditions where a mean flow is present.

Despite these subtle differences, the PVPM model provides a robust prediction of the resonance frequencies and also major features such as the sensitivity of the resonant frequency as a function of the liner porosity. These results demonstrate that the PVPM model is able to capture the attenuation effects of perforated liner absorbers where the acoustic signal propagates in parallel with the liner surface.

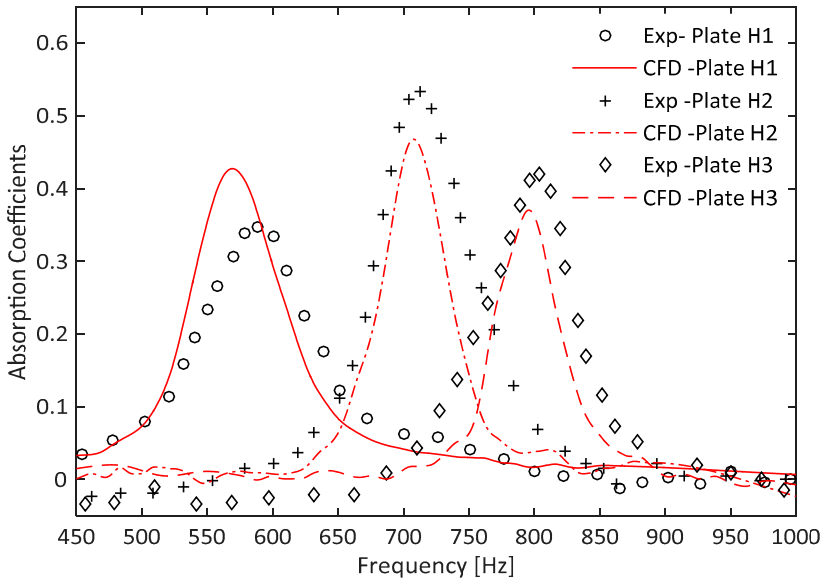

Figure 5. CFD and experimental comparison of absorption coefficients in sound grazing incidence conditions with closed cavity.

3.2. Grazing Acoustic Signal with Bias Flow

Experimental data by Eldredge and Dowling [21] are hereby cited to validate the PVPM model for the case of a grazing acoustic signal in the presence of a bias flow. Figure 6 illustrates the reported experimental configuration. Two 800 mm-long flow ducts were separated by a 178 mm-long double-layered perforated liner. Both liners were 3 mm thick. The outer liner was a 152 mm-diameter annular duct shell with 2% of its area perpendicularly perforated by 2.7 mm-diameter circular holes. The 127 mm-diameter inner liner was perforated by 0.75 mm-diameter circular holes, and the overall surface porosity was 4%. Those perforations on the inner liner were tilted 45° toward the downstream duct.

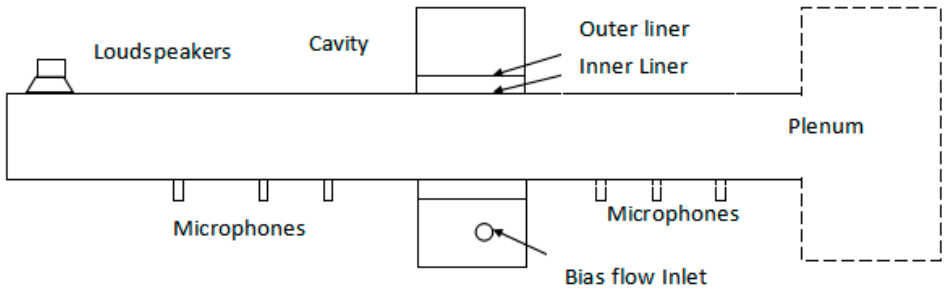

Figure 6. Test rig setup in the experiment by Eldredge and Dowling [21].

The axial region surrounding the two liners formed an inner air cavity. A bias flow was supplied to the cavity and the resultant mean flow with the duct exhausted to a large plenum at the exit of the downstream duct, as shown in Figure 6. This plenum was included in the computational domain in the following numerical simulations. Four loudspeakers were mounted at the end of the upstream flow duct, providing an acoustic signal ranging between 100 and 700 Hz. Transient pressure data were collected and processed by the four-microphone transfer function method as reported in Eldredge and Dowling [21].

The corresponding numerical simulations were carried out as part of this work, with the PVPM model representing the liner region, to obtain numerical results for acoustic absorption coefficients. The grid resolution is similar to that shown in Figure 4.

Absorption coefficients derived from the numerical simulations of this work, the experiments of Eldredge and Dowling [21] and also their derived model [21] are plotted against wave numbers at two different bias flow velocities in Figures 7 and 8. M_{in} stands

for the bias flow Mach number through the inner liner, k is the wave number of the noise signal and L is the length of the liner which is 178 mm. The results from the numerical simulations show very close agreement with both the experimental and model results. The variation in the absorption coefficient with the wave number is successfully captured by the PVPM model. This demonstrates that the combined CFD/PVPM model is able to successfully represent acoustic reflections from the downstream plenum.

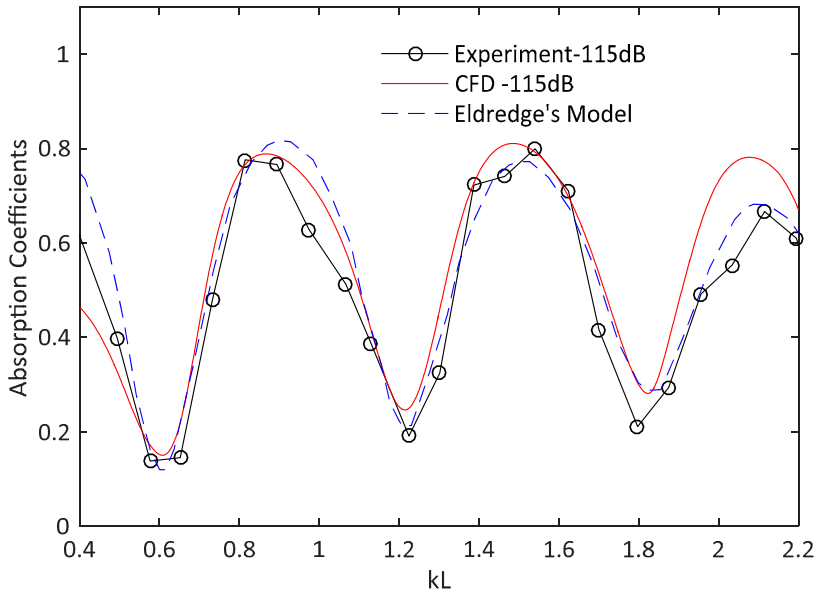

Figure 7. Numerical and experimental comparison of absorption coefficients at $M_{in} = 0.023$ and zero grazing flow conditions [21].

Despite the overall good agreement, differences of up to 11% do exist between the absorption coefficient curves acquired by the different methods, especially at very high frequencies when kL > 1.7. Eldredge and Dowling [21] suggested that this error may be a result of the high sensitivity of high-frequency signals to the interference between left- and right-traveling waves in the liner section.

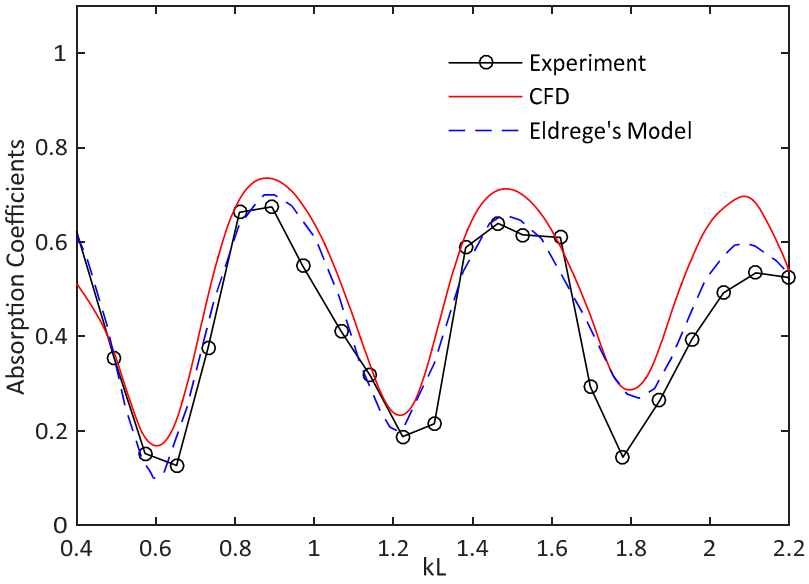

Figure 8. Numerical and experimental comparison of absorption coefficients at $M_{in} = 0.041$ and zero grazing flow conditions [21].

Figure 9 demonstrates how acoustic attenuation varies with the bias flow Mach number. All three methods suggest that the optimum absorption effect takes place between $0.01 < M_{in} < 0.02$, and all three methods indicate that a further increase in the bias flow speed above the optimum speed reduces the peak absorption coefficients. On the other hand, the minimum noise damping effect at frequencies $kL = 1.22$ is hardly changed by the bias flow speed. According to Eldredge and Dowling [21], the optimum attenuation effect of a perforated liner is achieved in the following bias flow condition:

$$\left(\frac{M_b}{\sigma}\right)_{opt} = \frac{s_l/s_d}{2\sqrt{2}} \tag{17}$$

where s_l is the area of the liner surface and s_d is the cross-section area of the flow duct. The optimum bias flow speed which yields the maximum damping effect depends on the porosity of the liner and its relative size to the flow duct, and it is accurately captured by the numerical method with the PVPM model.

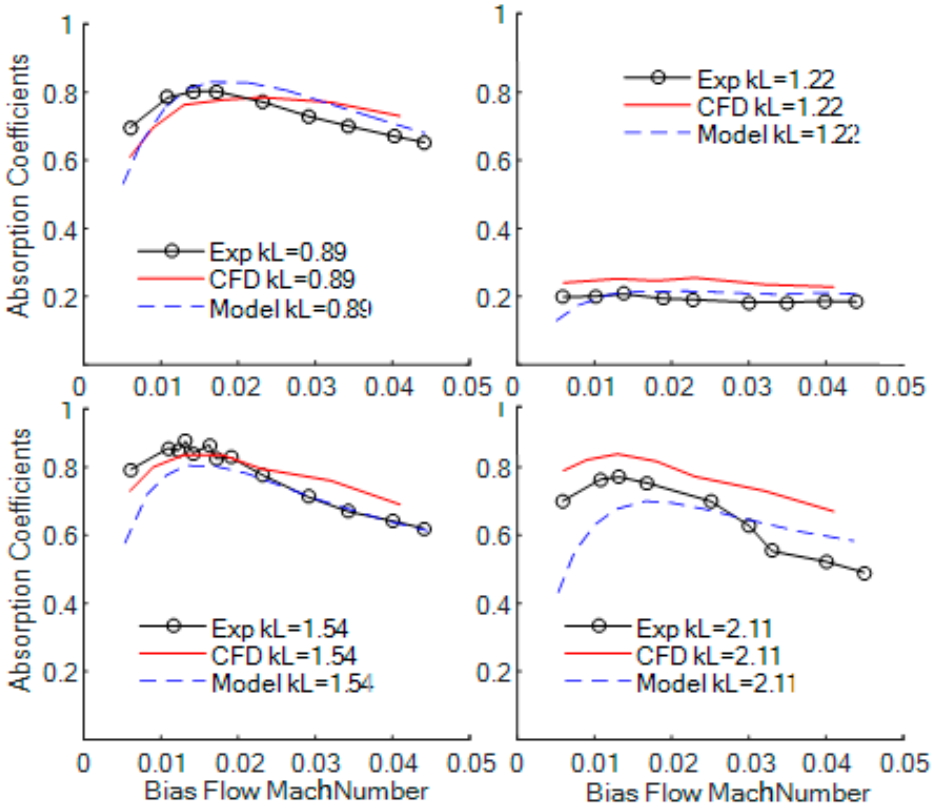

Figure 9. Numerical and experimental comparison of absorption coefficients variation with the bias flow speed in zero grazing flow conditions [21].

In conclusion, the numerical calculations, with the PVPM model representing the liner region, are able to accurately capture the noise damping effect of perforated liner absorbers where the noise signal travels in parallel with the liner surface and, at the same time, a bias flow is present.

3.3. Grazing Flow

Jing et al. experimentally investigated the effects of grazing flows on the acoustic impedance of four orifice liners [23]. Figure 10 illustrates the configuration of the test rig in the reported experiment, and Table 2 lists the geometric features of the orifice liners that were included in the tests. The grazing flow duct was a 120 × 120 mm square tube. A closed 150 mm-long, 35 mm-diameter cylindrical cavity was fixed on the side wall of the grazing flow duct. A loudspeaker was installed on the duct wall just opposite to the cavity. The sound signal was a sine signal of 200 Hz. Transient pressure data were collected and processed by the method described in Dean's work [48].

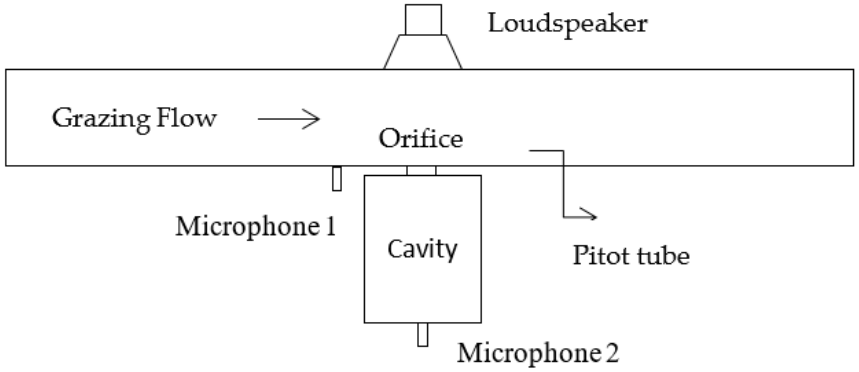

Figure 10. Test rig configuration for the investigation of grazing flow, Jing et al. [23].

Table 2. Geometric specifications of the orifice liners from the experiment by Jing et al. [23].

Liner No.	Hole Diameter (mm)	Liner Thickness (mm)	Number of Orifices	Porosity
JG1	3	2	4	2.94%
JG2	4.5	2	1	1.65%
JG3	7	0.5	1	4%
JG4	7	2	1	4%

CFD simulations of the experiments were obtained following the method described in Section 2. Acoustic impedances of the four orifice liners from the experiment of Jing [23] were obtained under various grazing flow conditions, with the PVPM model representing the liner region. Results from the derived normalized specific acoustic impedance from the numerical simulations are compared with experimental results in Figure 11. Both numerical and experimental methods suggest that the acoustic resistance r rises linearly with the grazing flow Mach number. More precisely, the experimental results indicate the linear proportional constant Cg to be 0.39, 0.41, 0.5 and 0.48 for liners JG1, JG2, JG3 and JG4, respectively. By comparison, the numerical results indicate 0.385, 0.417, 0.47 and 0.45 for these four liners, values which are in close agreement to the experimental values.

In addition, the simulation and experimental results are in close agreement in terms of the change in acoustic reactance with the grazing flow speeds. The difference between the experimental and numerical results is within 11% within the investigated grazing flow ranges. Both methods indicate that the magnitude of acoustic reactance x reduces with the rising grazing flow speeds, and the reduction tends to slow down at high grazing flow speeds. Therefore, the further developed PVPM model is able to represent acoustic impedance under the influence of grazing flows. Acoustic energy absorption coefficients are not shown here because the absorption data were not provided in the original experimental work [23].

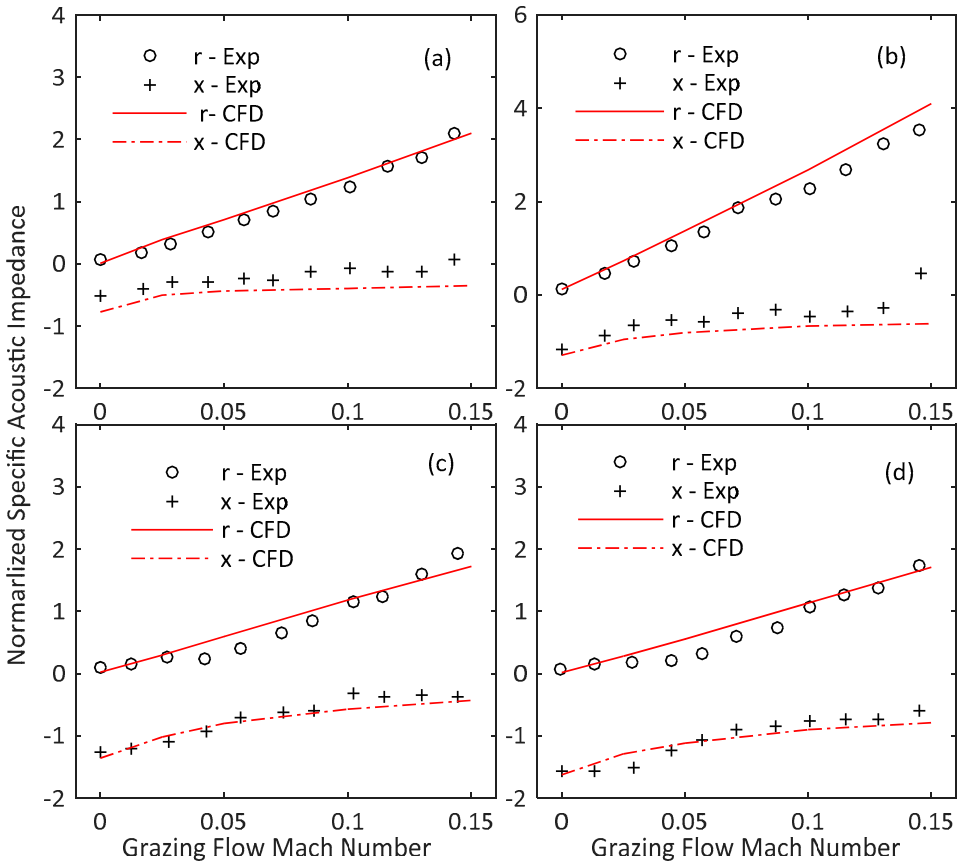

Figure 11. Numerical and experimental comparison of normalized specific acoustic impedance as a function of the grazing flow Mach number for (**a**) liner JG1, (**b**) liner JG2, (**c**) liner JG3 and (**d**) liner JG4 [23].

3.4. Simultaneous Grazing and Bias Flows

Grazing flows and bias flows coexist for perforated liner walls in gas turbine combustors. Therefore, the PVPM model must also be validated for those conditions in order to represent perforated liners in gas turbine engines.

Sun [22] experimentally investigated the effect of a simultaneous bias/grazing flow on the acoustic properties of perforated orifice liners. Figure 12 shows the test rig in the experiment by Sun [22]. A tube with a diameter of 35 mm was installed on the side walls of a grazing flow duct. A perforated orifice liner was installed between the two perpendicular ducts. An inlet was linked to the impedance tube through which the bias flow could be introduced in two ways: inflow and outflow. The inflow was introduced into the grazing flow duct, while the outflow was drawn out of the grazing flow duct. Only inflow cases are considered in this work because outflow cases are not realistic in gas turbine combustors. Geometric features of those three orifice liners from this experiment are listed in Table 3. A sine wave signal of 500 Hz was employed in all cases. Transient pressure data were collected and processed by the two-microphone transfer function method [32]. A numerical simulation of the experiment was obtained following the method described in Section 2.

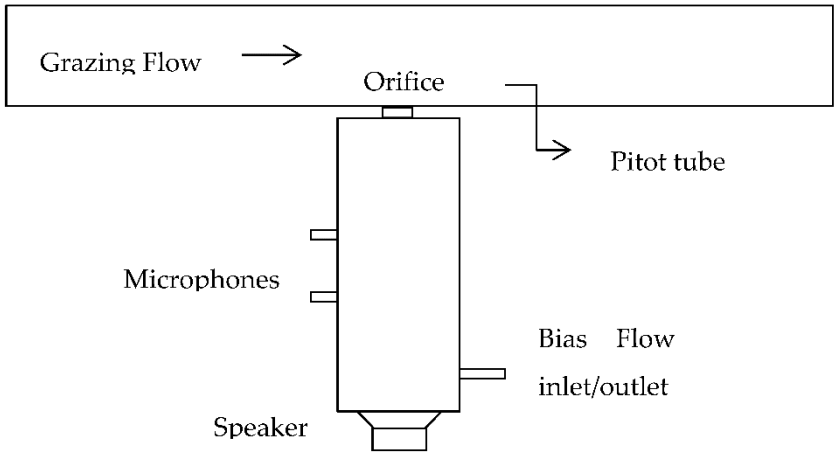

Figure 12. Test rig setup in experiment for the investigation of simultaneous bias/grazing flow effect, Sun et al. [22].

Table 3. Geometric specifications of the orifice liners, Sun et al. [22].

Liner No.	Hole Diameter (mm)	Liner Thickness (mm)	Number of Orifices	Porosity
JGB1	7	0.5	1	4%
JGB2	7	2	1	4%
JGB3	3	2	4	2.94%

A comparison of the normalized specific acoustic impedance of liners JGB1, JGB2 and JGB3 from the experiments by Sun et al. [22] under various simultaneous bias/grazing flow conditions is provided in Figures 13–15. First of all, all three figures show that acoustic resistance caused by the pure grazing flow rises with the grazing flow speeds, and the presence of the bias flow tends to reduce the impact of the grazing flow. Variations in acoustic resistance with the grazing flow speed are more obvious when the bias flow is very weak. For instance, when $M_b = 0.01$, the acoustic resistance of liner JGB1 increases by three times from approximately 0.6 at $M_g = 0$ to 1.9 at $M_g = 0.174$. However, when $M_b = 0.1$, the resistance only changes from 5.6 at $M_g = 0$ to 4.5 at $M_g = 0.174$. The change in acoustic resistance with the grazing flow speed is much less in the presence of a strong bias flow. The CFD results are also in satisfactory agreement with the experimental results under high-speed bias flow conditions. In these conditions, acoustic resistance and reactance are predominantly determined by the bias flow.

The experimental results indicate that the presence of a grazing flow tends to reduce the acoustic resistance in the case of a simultaneous bias/grazing flow, and this was referred to as the "negative grazing flow effect" in Sun's work [22]. However, the physical justification for this is not certain and is not included in the modified PVPM model. A comparison of the acoustic reactance is presented in Figures 13–15. In general, the effects of the simultaneous bias/grazing flow on the acoustic impedance of perforated liners are encouragingly reproduced by the PVPM model, despite a slight difference between the experiment and numerical results existing in those reactance curves.

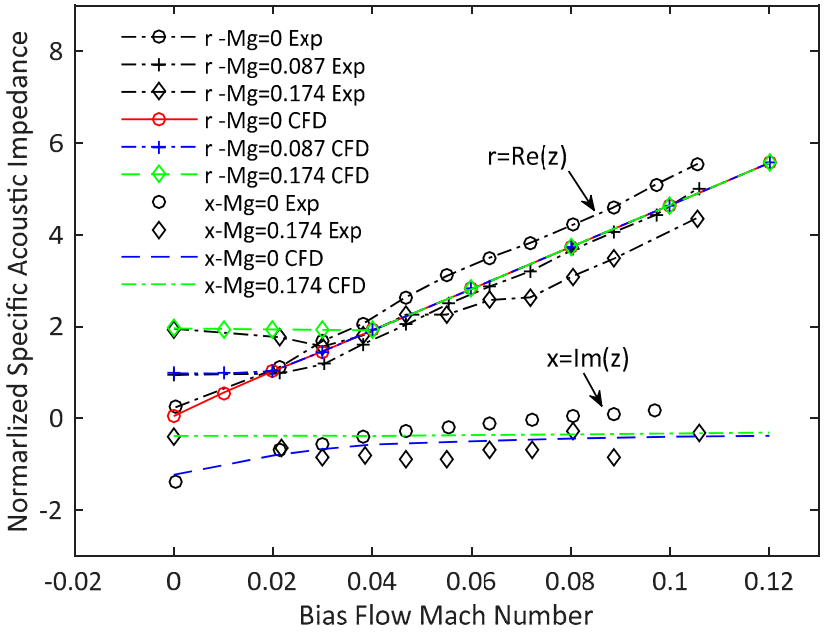

Figure 13. Numerical and experimental comparison of normalized specific acoustic impedance for liner JGB1 under various bias/grazing flow conditions [22].

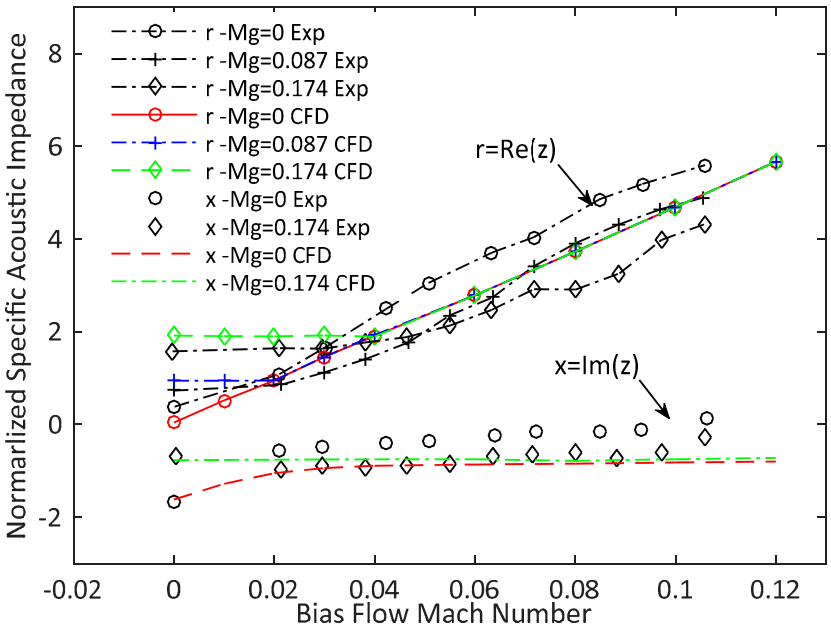

Figure 14. Numerical and experimental comparison of normalized specific acoustic impedance for liner JGB2 under various bias/grazing flow conditions [22].

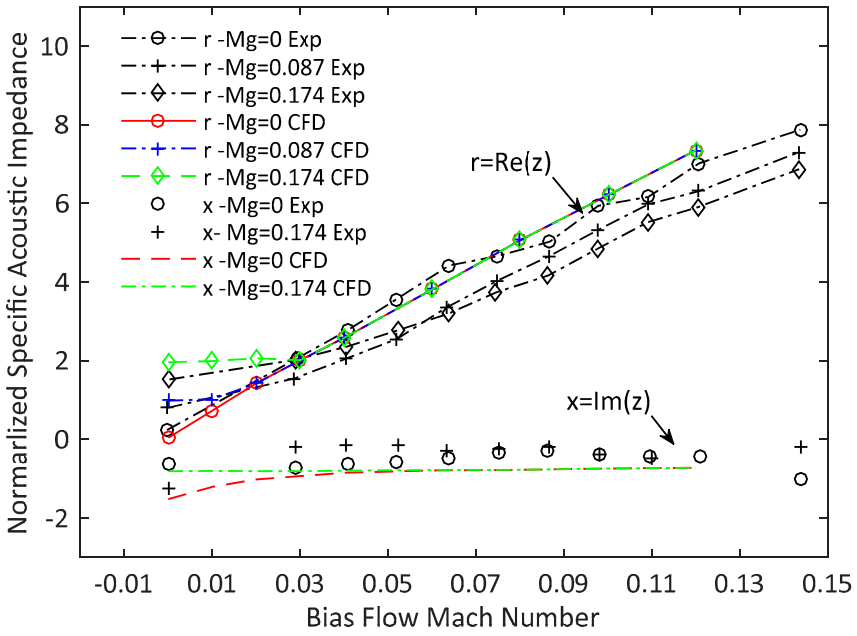

Figure 15. Numerical and experimental comparison of normalized specific acoustic impedance for liner JGB3 under various bias/grazing flow conditions [22].

3.5. Effects of Temperature of Grazing Flows

All previous validation case studies of the PVPM model were carried out at typical room temperatures. However, the industrial application of perforated liners typically involves high-temperature grazing flows. Experimental study of the effect of the flow temperature has received limited research [26,27].

Kabral [27] reported an experiment in which the acoustic impedance of a perforated liner was obtained in grazing flows at two different temperatures (295 K and 379 K). A 0.6 mm-thick liner was perforated by 23 ∅0.75 mm circular orifices. The perforated liner had an overall porosity of 16.3% and was backed by a 19 mm-deep air cavity. The cavity was made of 4 × 8 small square cavities, where each cavity unit had a cross-section of 6.9 × 6.9 mm. The perforated liner absorber was installed on the side wall of a 36 × 36 mm square grazing flow duct, as illustrated in Figure 16 [27]. A stepped sine wave was used with a frequency step of 50 Hz. Transient pressure data were collected and processed by the method described by Dean [48]. A numerical simulation of the experiment was obtained, again following the method described in Section 2.

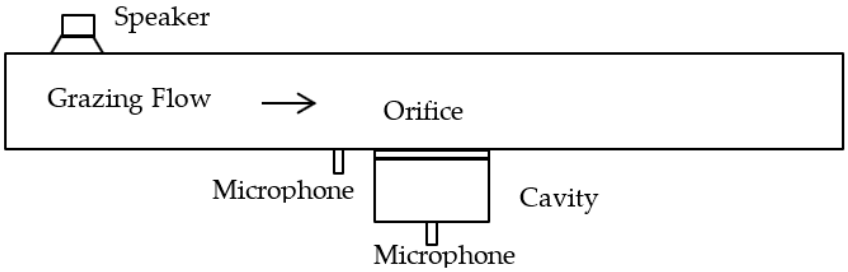

Figure 16. Schematic view of the test rig configuration in the experiment by Kabral [27].

Figures 17 and 18 present a comparison of the acoustic impedance between the simulations and the experiment for the perforated absorber. Acoustic impedances obtained by the PVPM model and the experiments agree closely in two different grazing flow conditions with the largest difference below 8%. Both the CFD simulations and experimental results suggest that the effect of the temperature on the normalized acoustic resistance is minor in the presence of grazing flows. The temperature of the grazing flow only changes the

acoustic reactance by translating acoustic reactance curves to higher frequencies. These findings are identical to those found in earlier experiments by Elnady [49], who showed that the influence of the ambient temperature on the acoustic resistance of perforated liners is rather weak, and only a high flow temperature modifies the acoustic impedance by shifting the reactance curves to high frequencies as a result of the changes in the speed of sound and the fluid density. The comparisons for this final validation case demonstrate that the PVPM model is able to represent the effects of temperature, at least at a moderate level, on the acoustic performance of perforated liners.

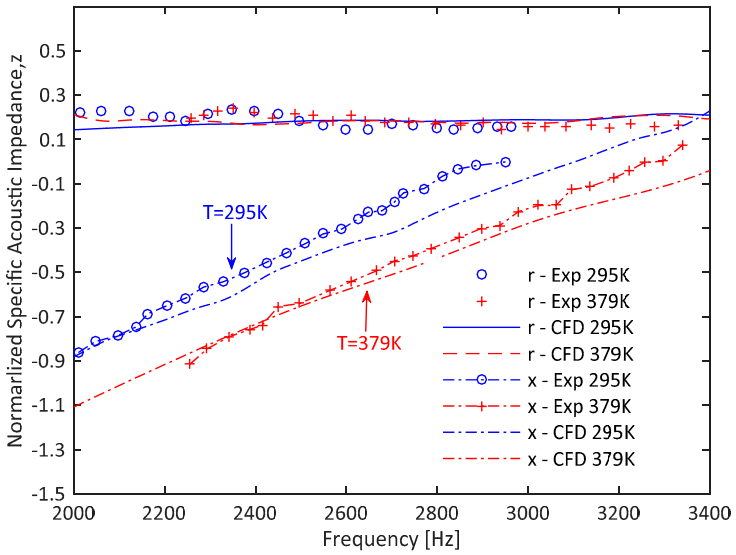

Figure 17. CFD and experimental comparison of normalized specific acoustic impedance ($M_g = 0.12$) [27].

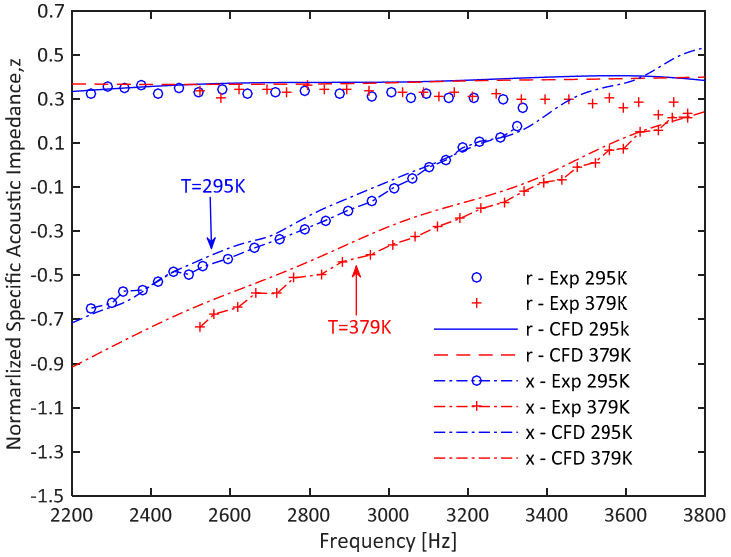

Figure 18. CFD and experimental comparison of normalized specific acoustic impedance ($M_g = 0.25$) [27].

4. Conclusions

The authors originally proposed that a physical velocity porous media model (PVPM model) was able to represent the acoustic attenuation of perforated liner absorbers. The model was validated against a number of well-established, well-cited experiments, for the case of when the acoustic signal was normal to the perforated plate, both with and without bias flows.

In this paper, the PVPM model was first further validated for situations where the acoustic signal is parallel to the perforated liner. The PVPM model was then further developed by including the effect of grazing flow-induced local resistance into the pressure loss source terms. The effective thickness of the porous media region for perforated liner representations was also improved to include the grazing flow effects. The further developed PVPM model was finally validated for situations where only a grazing flow is present, or when only a bias flow is present, and also situations where both bias flows and grazing flows coexist. The effects of grazing flow temperatures on the acoustic properties of perforated liners are also captured by the PVPM model with high accuracy.

Therefore, the PVPM model was validated in signal normal incidence scenarios, signal parallel incidence scenarios, pure grazing flows, pure bias flows, high-temperature grazing flows and also simultaneous bias and grazing flows. In all cases, the model provided excellent agreement with experimental data and can therefore be recommended for application to the simulation of the acoustic attenuation of perforated liner absorbers across a general range of industrial areas.

Author Contributions: Conceptualization, J.W. and P.R.; methodology, J.W.; software, P.R. and Q.Q.; validation, J.W., P.R. and Q.Q.; formal analysis, J.W.; investigation, P.R. and J.W.; resources, P.R. and Q.Q.; data curation, J.W.; writing—original draft preparation, J.W.; writing—review and editing, J.W., Q.Q. and P.R.; visualization, J.W.; supervision, P.R.; project administration, P.R. All authors have read and agreed to the published version of the manuscript.

Funding: This research received no external funding.

Institutional Review Board Statement: Not applicable.

Informed Consent Statement: Not applicable.

Data Availability Statement: The data presented in this study are available on request from the corresponding author. The data are not publicly available due to the sheer large size of the dataset.

Conflicts of Interest: The authors declare no conflict of interest.

References

1. Lieuwen, T.C.; Yang, V. (Eds.) *Gas Turbine Emissions*, 1st ed.; Cambridge University Press: Cambridge, UK, 2013; pp. 175–208.
2. Lieuwen, T.; Neumeier, Y.; Zinn, B.T. The role of un-mixedness and chemical kinetics in driving combustion instabilities in lean premixed combustors. *Combust. Sci. Technol.* **1998**, *135*, 193–211. [CrossRef]
3. Huang, Y.; Yang, V. Dynamics and stability of lean-premixed swirl-stabilized combustion. *Prog. Energ. Combust.* **2009**, *35*, 293–364. [CrossRef]
4. Steele, R.C.; Cowell, L.H.; Cannon, S.M.; Smith, C.E. Passive control of combustion instability in lean premixed combustors. *J. Eng. Gas Turbines Power* **2000**, *122*, 412–419. [CrossRef]
5. Noiray, N.; Durox, D.; Schuller, T.; Candel, S. Passive control of combustion instabilities involving premixed flames anchored on perforated plates. *Proc. Combust. Inst.* **2007**, *31*, 1283–1290. [CrossRef]
6. Zhao, D.; Li, Y. A review of acoustic dampers applied to combustion chambers in aerospace industry. *Prog. Aerosp. Sci.* **2015**, *74*, 114–130. [CrossRef]
7. Farmer, G.; Brown, D.; Rutherford, M.E. Preferential Multi-Hole Combustor Liner. U.S. Patent 6,655,149, 2 December 2003.
8. Wang, J.; Rubini, P.; Qin, Q.; Houston, B. A Model to Predict Acoustic Resonant Frequencies of Distributed Helmholtz Resonators on Gas Turbine Engines. *Appl. Sci.* **2019**, *9*, 1419. [CrossRef]
9. Lahiri, C. Acoustic Performance of Bias Flow Liners in Gas Turbine Combustors. Ph.D. Thesis, Technische Universität Berlin, Berlin, Germany, 2014.
10. Grace, S.M.; Horan, P.; Howe, S. The influence of shape on the Rayleigh conductivity of a wall aperture in the presence of grazing flow. *J. Fluids Struct.* **1998**, *12*, 335–351. [CrossRef]
11. Lee, D.; Kwon, Y. Estimation of the absorption performance of multiple layer perforated panel systems by transfer matrix method. *J. Sound Vib.* **2004**, *278*, 847–860. [CrossRef]
12. Houston, B.; Wang, J.; Qin, Q.; Rubini, P. Experimental and numerical investigation of Helmholtz resonators and perforated liners as attenuation devices in industrial gas turbine combustors. *Fuel* **2015**, *151*, 31–39. [CrossRef]
13. Jing, X.; Sun, X. Effect of plate thickness on impedance of perforated plates with bias flow. *AIAA J.* **2000**, *38*, 1573–1578. [CrossRef]
14. Jing, X.; Sun, X. Experimental investigations of perforated liners with bias flow. *J. Acoust. Soc. Am.* **1999**, *106*, 2436–2441. [CrossRef]

15. Rupp, J.; Carrotte, J.; Macquisten, M. The use of perforated damping liners in aero gas turbine combustion systems. *J. Eng. Gas Turbines Power* **2012**, *134*. [CrossRef]
16. Zhao, D.; Ang, L.; Ji, Z. Numerical and experimental investigation of the acoustic damping effect of single-layer perforated liners with joint bias-grazing flow. *J. Sound Vib.* **2015**, *342*, 152–167. [CrossRef]
17. Liu, J.; Herrin, W. Enhancing micro-perforated panel attenuation by partitioning the adjoining cavity. *Appl. Acoust.* **2010**, *71*, 120–127. [CrossRef]
18. Jing, X.; Sun, X. Sound-excited flow and acoustic nonlinearity at an orifice. *Phys. Fluids* **2002**, *14*, 268–276. [CrossRef]
19. Ingard, U.; Ising, H. Acoustic nonlinearity of an orifice. *J. Acoust. Soc. Am.* **1967**, *42*, 6–17. [CrossRef]
20. Tayong, R.; Dupont, T.; Leclaire, P. On the variations of acoustic absorption peak with particle velocity in micro-perforated panels at high level of excitation. *J. Acoust. Soc. Am.* **2010**, *127*, 2875–2882. [CrossRef]
21. Eldredge, D.; Dowling, P. The absorption of axial acoustic waves by a perforated liner with bias flow. *J. Fluid Mech.* **2003**, *485*, 307–335. [CrossRef]
22. Sun, X.; Jing, X.; Zhang, H.; Shi, Y. Effect of grazing–bias flow interaction on acoustic impedance of perforated plates. *J. Sound Vib.* **2002**, *254*, 557–573. [CrossRef]
23. Jing, X.; Sun, X.; Wu, J.; Meng, K. Effect of grazing flow on the acoustic impedance of an orifice. *AIAA J.* **2001**, *39*, 1478–1484. [CrossRef]
24. Kirby, R.; Cummings, A. The impedance of perforated plates subjected to grazing gas flow and backed by porous media. *J. Sound Vib.* **1998**, *217*, 619–636. [CrossRef]
25. Elnady, T.; Bodén, H.; Kontio, T. Impedance of SDOF perforated liners at high temperatures. In Proceedings of the 10th AIAA/CEAS Aeroacoustics Conference, Manchester, UK, 10–12 May 2004.
26. Rademaker, R.; Geurts, M. Hot-stream in-situ acoustic impedance measurements on various air-filled cavity and porous liners. *J. Aircr.* **2019**, *56*, 1–13.
27. Kabral, R. Determination of Liner Impedance under High Temperature and Grazing Flow Conditions. In Proceedings of the 20th AIAA/CEAS Aeroacoustics Conference, Atlanta, GA, USA, 16–20 June 2014.
28. Liu, J. Advanced Studies on Series Impedance in Waveguides with an Emphasis on Source and Transfer Impedance. Ph.D. Thesis, University of Kentucky, Lexington, KY, USA, 2011.
29. Dassé, J.; Mendez, S.; Nicoud, F. Large-eddy simulation of the acoustic response of a perforated plate. In Proceedings of the 14th AIAA/CEAS Aeroacoustics Conference, Vancouver, BC, Canada, 5–7 May 2008.
30. Fan, W.; Guo, X. An Investigation of Acoustic Attenuation Performance of Silencers with Mean Flow Based on Three-Dimensional Numerical Simulation. *Shock. Vib.* **2016**, *2016*, 6797593. [CrossRef]
31. Liu, C.; Ji, Z. Computational fluid dynamics-based numerical analysis of acoustic attenuation and flow resistance characteristics of perforated tube silencers. *J. Vib. Acoust.* **2014**, *136*. [CrossRef]
32. Wang, J.; Rubini, P.; Qin, Q. Application of a porous media model for the acoustic damping of perforated plate absorbers. *Appl. Acoust.* **2017**, *127*, 324–335. [CrossRef]
33. ANSYS. *Ansys Fluent 17.2. Theory Guide. Chapter 21: Solver Theory*; ANSYS, Inc.: Canonsburg, PA, USA, 2013.
34. Fok, W. Theoretical study of the conductance of a circular hole in a partition across a tube. *Dokl. Akad. Nauk. SSSR* **1941**, *31*, 875–882.
35. Tonon, D.; Moers, E.; Hirschberg, A. Quasi-steady acoustic response of wall perforations subject to a grazing-bias flow combination. *J. Sound Vib.* **2013**, *332*, 1654–1673. [CrossRef]
36. Rice, J. Theoretical study of the acoustic impedance of orifices in the presence of a steady grazing flow. *J. Acoust. Soc. Am.* **1976**, *59*. [CrossRef]
37. Syed, A.; Yu, J.; Kwan, W.; Chien, E.; Jones, G. *The Steady Flow Resistance of Perforated Sheet Materials in High-Speed Grazing Flows*; NASA: Cincinnati, OH, USA, 2002.
38. Rao, N.; Munjal, L. Experimental evaluation of impedance of perforates with grazing flow. *J. Sound Vib.* **1986**, *108*, 283–295.
39. Bauer, B. Impedance theory and measurements on porous acoustic liners. *J. Aircr.* **1977**, *14*, 720–728. [CrossRef]
40. Heidelberg, J.; Rice, L. *Experimental Evaluation of a Spinning-Mode Acoustic-Treatment Design Concept for Aircraft Inlets*; NASA: Cleveland, OH, USA, 1980.
41. Rice, J. *A Model for the Acoustic Impedance of a Perforated Plate Liner with Multiple Frequency Excitation*; NASA: Cleveland, OH, USA, 1971.
42. Dean, D.; Tester, J. *Duct Wall Impedance Control as an Advanced Concept for Acoustic Impression*; NASA: Marietta, GA, USA, 1975.
43. Elnady, T.; Boden, H. On semi-empirical liner impedance modelling with grazing flow. In Proceedings of the 9th AIAA/CEAS Aeroacoustics Conference and Exhibit, Hilton Head, SC, USA, 12–14 May 2003.
44. Kooi, W.; Sarin, S.L. An experimental study of the acoustic impedance of Helmholtz resonator arrays under a turbulent boundary layer. In Proceedings of the 7th Aeroacoustics Conference, Palo Alto, CA, USA, 5–7 October 1981.
45. Kaji, S.; Hiramoto, M.; Okazaki, T. Acoustic characteristics of orifice holes exposed to grazing flow. *Bull. JSME* **1984**, *27*, 2388–2396. [CrossRef]
46. Poinsot, J.; Lelef, K. Boundary conditions for direct simulations of compressible viscous flows. *J. Comput. Phys.* **1992**, *101*, 104–129. [CrossRef]

47. Selle, L.; Nicoud, F.; Poinsot, T. Actual impedance of non-reflecting boundary conditions: Implications for computation of resonators. *AIAA J.* **2004**, *42*, 958–964. [CrossRef]
48. Dean, D. An in-situ method of wall acoustic impedance measurement in flow ducts. *J. Sound Vib.* **1974**, *34*, 97–130. [CrossRef]
49. Elnady, T. Modelling and Characterization of Perforates in Lined Ducts and Mufflers. Ph.D. Thesis, KTH Royal Institute of Technology, Stockholm, Sweden, 2004.